This is a preprint, the final version is subject to change, of the American Mineralogist (MSA)
Cite as Authors (Year) Title. American Mineralogist, in press.
(DOI will not work until issue is live.) DOI: http://dx.doi.org/10.2138/am-2017-6172

REVISION 1

The solubility of $CePO_4$ monazite and YPO_4 xenotime in KCl-H_2O fluids at 800°C and 1.0 GPa: Implications for REE transport in high-grade crustal fluids

Philipp Mair [1], Peter Tropper [1], Daniel E. Harlov [2,3], Craig E. Manning [4],

[1]Institute of Mineralogy and Petrography, Faculty of Geo- and Atmospheric Sciences, University of Innsbruck, Innrain 52f, A-6020 Innsbruck, Austria

[2]Helmholtz Zentrum Potsdam, Deutsches GeoForschungsZentrum, Telegrafenberg, D-14473 Potsdam, Germany

[3]Department of Geology, University of Johannesburg, P.O. Box 524, Auckland Park, 2006 South Africa

[4]Department of Earth and Space Sciences, University of California, Los Angeles, CA 90095-1567, USA

Abstract

Monazite ($CePO_4$) and xenotime (YPO_4) are important hosts for REE, and thus can be used to monitor REE mass transfer in a variety of settings. In this investigation, the solubilities of synthetic monazite and xenotime were measured in KCl-H_2O fluids at 800°C and 1.0 GPa, using the piston-cylinder apparatus. The experimental results indicate an increase in monazite and xenotime solubility in aqueous fluids with moderate KCl mole fractions (X_{KCl}) in agreement with previous investigations of the solubility of these phases in NaCl-H_2O. Under all conditions, monazite and xenotime dissolve congruently. The solubility of synthetic monazite increases from 8 ppm in pure H_2O to 335 ppm at $X_{KCl} = 0.506$. The solubility of synthetic xenotime rises from 46 ppm in pure H_2O to 126 ppm at $X_{KCl} = 0.348$, above which it is constant or declines slightly. Monazite and xenotime solubilities are considerably lower in KCl-H_2O than in NaCl-H_2O at the same salt concentration. Best fit equations for the solubilities of the two phases are:

$$c_{mz} = -464\ X^{2}_{KCl} + 891\ X_{KCl} + 8$$

and

This is a preprint, the final version is subject to change, of the American Mineralogist (MSA)
Cite as Authors (Year) Title. American Mineralogist, in press.
(DOI will not work until issue is live.) DOI: http://dx.doi.org/10.2138/am-2017-6172

$c_{xt} = -563\ X^2_{KCl} + 432\ X_{KCl} + 46$

where mz and xt stand for monazite and xenotime, and $X_{KCl} = n_{KCl} / (n_{KCl} + n_{H2O})$ where n is moles. The change in solubilities with KCl implies that Ce dissolves as an anhydrous chloride complex ($CeCl_3$), whereas Y forms a mixed Cl-OH solute ($YCl(OH)_2$). The data also imply that H_2O-NaCl fluids and H_2O-KCl fluids close to neutral pH can transport substantial amounts of REE and Y, thus obviating the need to invoke low pH solutions in high-grade environments where they are highly unlikely to occur.

Keywords: Monazite, Xenotime, Solubility, Experimental petrology, REE mobility, Metamorphic fluids, Brines

Introduction

Aqueous fluids are responsible for substantial mass transfer in high pressure (P) and temperature (T) environments. Understanding the scale and magnitude of fluid-mediated compositional change is central to many studies of magmatic and metamorphic systems and ore deposits such as REE-enriched iron oxide-apatite deposits (cf. Harlov et al., 2016) or REE-enriched carbonatites (e.g., Yang et al., 2003). For example, lithologies transported to deep-crustal conditions along Barrovian P-T paths show evidence for significant compositional modification by metamorphic fluids (e.g., Ague, 1994a,b). Similarly, in subduction zones, slab devolatilization generates a fluid phase that is capable of major metasomatic activity (e.g., Manning, 2004). High-pressure (P) and temperature (T) environments (e.g., Barrovian and granulite metamorphism, and subduction zones) often record evidence of mobilization of elements that show very low solubility in H_2O, such as Al, Ti, and rare-earth elements (REE). Explanations may involve extremes in pH or complexing with halogens, alkalis, or both or polymerization with alkalis, Al and Si (e.g., Manning, 2004; Newton and Manning, 2010; Tropper et al., 2011; Tropper et al., 2013). A number of observations point to the participation of brines in high-grade metamorphic processes. These include not only findings of alkali and alkaline-earth halides as daughter crystals in fluid inclusions, but also

appreciable concentrations of Cl measured in minerals from high-grade rocks such as amphiboles, biotite, scapolite and apatite, and direct observations on high-temperature halides present in the intergranular space in high-grade rocks (e.g. Aranovich et al., 2014). Saline fluids may also be important in subduction-zone metasomatism (Barnes et al., 2017; Keppler, 2017).

Accessory minerals are minor in abundance, but can contain elements as major components (for example Ce in monazite and Y in xenotime), which with respect to the whole rock would be considered trace elements. If these minerals are part of the solid assemblage, their solubility will govern the abundance of key trace elements in co-existing fluids, including Ti, Nb, Ta, Zr, Hf, and REE. Therefore knowledge of rare earth element (Y+REE) redistribution during high-grade metamorphism is of fundamental importance in determining the origin of typical light (L)REE-enrichment of calc-alkaline magmas, commonly ascribed to the metasomatic effects of a subducting slab on the overlying mantle wedge (e.g., Ionov and Hofmann, 1995; Rubatto and Hermann, 2003; Gao et al., 2007). It is therefore essential to understand the behavior of (Y+REE) carriers such as monazite and xenotime during that metasomatic processes that attend high-grade metamorphism and subduction.

Monazite and xenotime are important accessory phases in metamorphic and igneous rocks (e.g., Spear and Pyle, 2002). Occurring over a range of metamorphic lithologies, settings, and P-T conditions, these phosphates have great utility as prograde index minerals that can be used for geochronology (e.g., Harrison et al., 2002) and geothermometry (e.g., Gratz and Heinrich, 1997; Janots et al., 2008). They represent important reservoirs for light (LREE) and heavy (Y+HREE) rare earth elements. The exchange of (Y+REE) between orthophosphates and silicates, such as garnet, provides information concerning the P-T history of metamorphic terranes (e.g., Spear and Pyle, 2002). Y+REE orthophosphates also play an important role in controlling the distribution of (Y+REE), U, and Th during granitoid crystallization (e.g., Montel, 1993). Their high durability and resistance to metamictization make the (Y+REE) phosphates potential hosts for nuclear waste disposal (e.g., Ewing, 2001). The mobility of REE in crustal and mantle fluids are especially important because of their role in REE ore-deposit formation (e.g., Williams-Jones et

al., 2012; Harlov et al., 2016) as well as their contribution in tracing magmatic (e.g., Markl and Piazolo, 1998; Agangi et al., 2010) and metamorphic (e.g., Yardley, 1985; Brennan, 1993) petrogenetic processes. Potassium metasomatism has been recognized by field workers in high-grade metamorphic terranes for over a century (e.g. Billings, 1938). Alkali exchange in natural feldspars (K-feldspathization) gives rise to ‘‘replacement antiperthite’’, a common texture in high-grade gneisses (Todd and Evans, 1994; Hansen et al., 1995). Potassium species are also important constituents of high-grade metamorphic fluids (e.g., Aranovich and Newton, 1997; Newton et al., 1998; Harlov and Förster, 2002a; Harlov, 2012) and potassium metasomatism has been recognized in high-grade metamorphic terranes (e.g., Hansen et al., 1995; Newton et al., 1998; Harlov et al., 1998; Harlov and Förster, 2002a; Harlov, 2012). KCl brines or K-rich also act as metasomatic fluids in xenoliths from the lower crust and upper mantle (Harlow and Davies, 2004), Kimberlites (Kamenetsky et al., 2004), as well as brine-rich inclusions in diamonds (Tomlinson et al., 2004). Sylvite (KCl) has been identified as a daughter mineral in some of the concentrated brine inclusions which have been described with increasing frequency in many petrogenetic settings, including granites (Dunbar et al., 1996), gabbros (Pasteris et al., 1995), high-grade gneisses (Touret, 1985), carbonatites (Sampson et al., 1995), eclogites (Philippot and Selverstone, 1991), and the super-high-pressure coesite-bearing metasediments (Philippot et al., 1995). KCl is thought to have been a major solute of the complex saline fluids which produced regional metasomatism and metal ore segregation in Cloncurry, Queensland (DeJong and Williams, 1995) and the Melones Fault Zone of California (Albino, 1995). The role of KCl-NaCl-H_2O-rich fluids has also been investigated in a number of experimental studies on the relationship between activity and concentration (Aranovich and Newton, 1997), the stability of phlogopite (Aranovich and Newton, 1998), fluid-induced dehydration of tonalites (Harlov, 2004; Harlov et al., 2006) and biotite-amphibole gneiss (Safonov et al., 2012), monazite/apatite dissolution-reprecipitation (Harlov and Förster, 2003; Harlov et al., 2005), quartz solubility (Shmulovich et al., 2005), and brine-assisted anataxis (Aranovich et al., 2014).

Despite their importance as minerals whose occurrence as prograde index minerals can be coupled with

geochronology (e.g. Janots et al., 2009) and their economic importance (Williams-Jones et al., 2012; Harlov et al., 2016), little is known about the solubility systematics of two of the most important orthophosphate REE-bearing minerals, monazite ($CePO_4$-) and xenotime (YPO_4-) in aqueous fluids of various compositions at high P (> 0.5 GPa) and T (> 300 °C). It is therefore essential to understand their solubility behavior with respect to P-T-X_i conditions and complexation during metasomatic processes that attend high-grade crustal metamorphism and crustal/mantle/rock-fluid interactions occurring during subduction.

Experimental methods

Solubility experiments involving solutions with varying concentrations of KCl were conducted on synthetic crystals of monazite ($CePO_4$) and xenotime (YPO_4), and natural monazite from a beach sand in Cleveland Co., North Carolina (UCLA mineral collection #MS 1762), which contains 59.96 wt% LREE (29.41 wt% Ce_2O_3, 13.44 wt% La_2O_3, 11.15 wt% Nd_2O_3, 3.08 wt% Pr_2O_3, 1.87 wt% Sm_2O_3 and 1.01 wt% Gd_2O_3) and 0.76 wt% HREE (with 0.55 wt% Y_2O_3, 0.08 wt% Dy_2O_3, 0.07 wt% Tb_2O_3, 0.02 wt% Ho_2O_3, 0.02 wt% Er_2O_3 and 0.02 wt% Yb_2O_3) (Tropper et al., 2011).

Synthetic crystals of monazite ($CePO_4$) or xenotime (YPO_4) were synthesized by mixing stoichiometric amounts of $REE(NO_3)*6H_2O$ and $(NH_4)_2HPO_4$ in solution. The resulting precipitate was allowed to settle and the excess fluid poured off. The precipitate was then dried and ground. Twenty grams of Pb-free flux (Na_2CO_3:MoO_3 = 1:3) mixed with 0.8 g precipitate was packed in a Pt crucible with a loose cover and heated to 1280 °C. The molten flux was allowed to equilibrate at 1280 °C for 15 h, and then cooled to 870 °C at 3 °C per hour (Cherniak et al., 2004; Tropper et al., 2011). The resulting transparent, light brownish yellow, euhedral to semi-euhedral monazite and xenotime crystals range from 0.1 mm to 2 mm in diameter. The smaller crystals are inclusion-free, but some of the larger crystals (> 1 mm) contain scattered melt inclusions.

Single crystals, optically free of flux melt inclusions, were selected for use in the solubility studies. Each crystal was first ground into spherical shapes with a diameter of ~ 1 – 2 mm using 400-grit emery paper to remove sharp edges, and then rolled in 800-grit emery paper until they acquired a polish. The polished crystals were cleaned in ethanol in an ultrasonic bath, and then dried at 120 °C for 15 min. This procedure generated single crystals that ranged in weight from 0.7 to 3.0 mg (Table 1). Each experiment consisted of an outer Pt capsule (outer diameter: 3.0 mm, thickness: 0.2 mm) and an inner Pt capsule (outer diameter: 2.0 mm, thickness: 0.1 mm) in which the monazite or xenotime single crystal was placed. Thick-walled Pt (0.2 mm) was used for the outer capsule to minimize puncturing by the thermocouple. The use of an inner capsule protected the crystal and minimized thermal gradients in the capsule (Tropper and Manning, 2005). After inserting the crystal, the inner capsule was lightly crimped to facilitate H_2O penetration while ensuring crystal containment during the experiments. The inner Pt capsule, plus precisely weighed quantities of KCl and H_2O (Table 1), were then placed in the outer Pt capsule. The outer Pt capsule was sealed by arc-welding and then placed in a 120 °C oven for 30 min to check for leakage.

All experiments were performed at 800 °C and 1000 MPa in a non end-loaded piston-cylinder apparatus, using 22 mm diameter NaCl assemblies with a cylindrical graphite oven and sealed by pyrophyllite rings. Each double capsule assembly was placed horizontally at the center of the NaCl assembly surrounded by the graphite-furnace and packed in NaCl. It was covered with a small, thin pyrophyllite sheet to help prevent puncture by the thermocouple which is in direct contact with the Pt capsule. Pressure and temperature was monitored using a pressure gauge and a NiCr-Ni thermocouple, respectively. Pressure was maintained to within 200 bar gauge pressure and the accuracy of the reported temperature is estimated to be ± 2 °C. Each experiment was initially brought to 0.2 GPa and 100 °C and held for 15 min, then brought to 800 °C and 1.0 GPa following a temperature and pressure ramp of 20 °C/min and 0.02 GPa/min. After 12 h, the experiments were quenched to $T < 150$ °C and $P < 0.6$ GPa within several seconds by shutting off the power to the graphite oven. Run times of 12 h for each experiment at 800 °C and 1.0 GPa were assumed sufficient to ensure significant reaction and equilibration of the monazite or

xenotime starting crystals with the solution. Attainment of constant solubility within 12 h is consistent with equilibration rates in other solubility measurements at high T and P, based on previous studies (e.g., Caciagli and Manning, 2003; Tropper and Manning, 2005; Tropper et al., 2011).

After each experiment, the outer capsule was pierced with a needle, and the pH of the quench fluid was checked with a pH-indicator paper with an accuracy of < 0.5 pH units (Table 1). After drying for 30 min at 120 °C, the monazite or xenotime crystal was then extracted from the inner capsule, treated ultrasonically in ethanol to remove adhering quench precipitate, dried at 120 °C, and weighed with a Mettler Toledo XP2U ultra-microbalance ($1\sigma = 0.1$ µg) (Table 1). All monazite and xenotime grains were then examined optically with a binocular microscope. Single crystals from selected experiments were mounted onto double-sided carbon tape and characterized by a JEOL JSM-6010LV scanning electron microscope (SEM) equipped with a Quantax EDS (Bruker).

The solubility of monazite and xenotime is reported in parts/million by weight (ppm), and is calculated via the formulas $(\Delta m_{mz} / H_2O + KCl + \Delta m_{mz}) * 10^6$ and $(\Delta m_{xt} / H_2O + KCl + \Delta m_{xt}) * 10^6$, where mz and xt stand for monazite and xenotime. Reported mole fractions of KCl (X_{KCl}) were calculated from the starting ratio $n_{KCl} / n_{KCl} + n_{H2O}$ in the experiment. KCl and H_2O masses were determined on a Mettler Toledo AX205 DeltaRange microbalance (1σ = 0.03 mg) (Table 1). For further speciation calculations the monazite and xenotime mass loss (Δm_{mz} and Δm_{xt}) and the measured pH were used to calculate ionic species utilizing the concept of the limiting reactant (Table 2a, Table 2b).

Results

Textures and equilibrium

The experimental results are given in Table 1. Run products included partly dissolved starting monazite- (Fig. 1a) and xenotime crystals (Fig. 1c), recrystallized $CePO_4$ grains on the surface of monazite starting crystals (Fig. 1b), yttrium chloride crystals on the surface of xenotime starting crystals (Fig. 1d), newly formed secondary monazite- (Fig. 2a, Fig. 2b), xenotime- (Fig. 2c, Fig. 2d), and yttrium chloride crystals

(Fig. 2c) in the outer capsules of some experiments, and a sub-micron sized white powder consisting of KCl (Fig. 2). The chemical identification of the yttrium chloride crystals was done semi-quantitatively using EDS analysis on the scanning electron microscope (SEM). Despite the small grain size and their adherence to the crystal faces of the starting crystals EDS analysis showed distinct Y and Cl peaks only and based on the approximate ratio between Y and Cl of 1:1, we infer the stoichiometry of this compound to be $YCl(OH)_2$. This quench phase most likely formed from the strongly hygroscopic phase YCl_3, which reacts directly with H_2O to $YCl(OH)_2$ and HCl based on the following chemical reaction: 1 YCl_3 + 2 H_2O = 1 $YCl(OH)_2$ + 2 HCl (Klevtsova & Klevtsov, 1965; Haschke, 1975; Zhuravleva et al., 2013). Tropper et al. (2011) postulated for the system xenotime-H_2O-NaCl that a similar simple equilibrium could account for this relationship namely: $YPO_4 + NaCl + 2H_2O = YCl(OH)_2 + NaH_2PO_4$. The residual monazite- and xenotime crystals displayed solution-rounded edges (Fig. 1a, Fig. 1c) and in some cases, significant dissolution grooves (Fig. 1a). The recrystallized $CePO_4$ grains on the surface of the monazite starting crystals occur as idiomorphic, prismatic, tabular – granular aggregates (Fig. 1b) and quench crystals occur as tiny, round precipitates, which were distributed randomly on the surface of the xenotime starting crystals (Fig. 1d). The newly formed euhedral secondary monazite and xenotime crystals occur as hollow, prismatic needles (Fig. 2), which are randomly distributed throughout the inner and outer capsules. The abundance of secondary monazite and xenotime needles increased with increasing X_{KCl}, accompanied by an increase in monazite or xenotime solubility (Table 1). The size of the secondary monazite crystals was up to ~ 15 µm along the c-axis (Fig. 2a, Fig. 2b), the size of the secondary xenotime crystals was up to ~ 5 µm along the c-axis (Fig. 2c, Fig. 2d). Both secondary monazite and xenotime crystals vary from sparse and separate crystallites to fibrous aggregates which were mostly embedded in KCl aggregates (Fig. 2). Two generations of secondary monazite quench crystals with different size and morphology (Fig. 2b) were found in the system monazite-H_2O-KCl at a mole fraction of $X_{KCl} = 0.1$. The first generation of monazites (sec mz I) can be recognized by its characteristic prismatic crystals (Fig. 2a, Fig. 2b). The second generation of monazites (sec mz II) occurs as stellate clusters of thin needles, which are

200 significantly smaller than the monazite crystals of the first generation. In addition to the secondary
201 monazite and xenotime crystals, < 2 μm tabular – prismatic grains of $YCl(OH)_2$ crystals were observed in
202 the system xenotime-H_2O-KCl at a mole fraction of $X_{KCl} = 0.1$, embedded in KCl aggregates (Fig. 2c).
203 Based on the textural observations, it can be assumed that the newly formed secondary monazite,
204 xenotime, and yttrium chloride crystals nucleated and grew during quenching to room temperature from
205 the experimental T, whereas the KCl aggregates precipitated during drying after initial puncturing of the
206 outer capsule. The attribution of these secondary phases as quench material is in accordance with previous
207 observations from similar experiments (e.g., Tropper and Manning, 2005, 2007a,b; Antignano and
208 Manning, 2008, Tropper et al., 2011). No evidence for vapor-transport of monazite or xenotime was
209 observed, unlike in some mineral-fluid systems such as calcite, rutile, and corundum (Caciagli and
210 Manning, 2003; Tropper and Manning, 2005, 2007b) or fluorapatite in the system NaCl + H_2O (Antignano
211 and Manning, 2008).
212
213 **Monazite solubility in H_2O-KCl**
214 The experimental results in the system monazite-H_2O-KCl are given in Table 1 and shown in Fig. 3a. At
215 800 °C and 1.0 GPa, the solubility of the synthetic monazite in pure H_2O is 8 ppm (Table 1) (Tropper et
216 al., 2011). The solubilities of synthetic monazite in H_2O-KCl fluids indicate an increase in the dissolved
217 monazite concentration with rising X_{KCl} from 78 ± 4 ppm ($X_{KCl} = 0.101$) to 335 ± 3 ppm ($X_{KCl} = 0.506$
218 (Table 1). The data on the variation in synthetic monazite solubility with X_{KCl} at 1.0 GPa and 800 °C (Fig.
219 3a) can be fit to a second-degree polynomial function using least squares regression:

220 $$c_{mz} = -464\ X^2_{KCl} + 891\ X_{KCl} + 8 \qquad (1)$$

221 where c_{mz} is the solubility of the synthetic monazite in ppm ($R^2 = 0.986$) and X_{KCl} is the mole fraction of
222 KCl. It can be also seen from Figure 3a that at $X_{KCl} = 0.262$, the solubility of natural monazite (186 ± 3
223 ppm) (Table 1) fits well to the data of synthetic monazite solubility. In contrast to the H_2O-KCl system,
224 monazite solubilities are considerably higher in the H_2O-NaCl system as shown by Tropper et al. (2011).

Their results also indicate an increase in the dissolved monazite concentration with rising X_{NaCl} to near halite saturation from 152 ppm (X_{NaCl} = 0.092) to 442 ppm (X_{NaCl} = 0.498) (Fig. 3a). The increase in the $CePO_4$ solubility with increasing NaCl concentration is similar to that seen for apatite, fluorite, calcite, anhydrite (Antignano and Manning, 2008; Tropper and Manning, 2007a; Newton and Manning, 2002; Newton and Manning, 2005) and monazite in the system H_2O-KCl. In addition, the quench pH of the aqueous solutions in the monazite-H_2O-KCl experiments was 7.0 – 7.5 (Table 1).

Figure 4 and Figure 5 show the relationship between the molality of monazite vs. the mole fraction of KCl (X_{KCl}) and the activity of H_2O at 800°C and 1.0 GPa. The molality of the monazite is reported in mol/kg, and is calculated from the amount of substance (n_{mz}) divided by the mass of H_2O + KCl. The H_2O and KCl activities were calculated using the Aranovich and Newton (1996, 1997) NaCl-KCl a-*X* formulation. Aranovich and Newton (1997) found that the KCl component lowers a_{H2O} even more than NaCl at a given T, P, and X_{H2O}, and that the KCl activity is lower for a given salt concentration than the NaCl activity (Aranovich and Newton, 1996). At 1.0 GPa, the solutions closely approach an ideal fused salt mixture, where the activities of H_2O and KCl correspond to an ideal activity formulation. The low H_2O activity at high pressures in concentrated KCl solutions indicates that such solutions should be feasible as chemically active fluids capable of coexisting with solid rocks in many deep crustal and upper mantle metamorphic and metasomatic processes (Aranovich and Newton, 1996).

Xenotime solubility in H_2O-KCl

The experimental results for the system xenotime-H_2O-KCl are given in Table 1 and shown in Fig. 3b. In pure H_2O at 800°C and 1.0 GPa, the solubility of synthetic xenotime is 46 ppm (Table 1) and is thus ~ 6 times higher than for synthetic monazite (8 ppm) (Table 1; Tropper et al., 2011). The solubilities of synthetic xenotime in H_2O-KCl fluids show an increase in the dissolved xenotime concentration with X_{KCl} increasing from 67 ± 5 ppm (X_{KCl} = 0.099) to 126 ± 4 ppm (X_{KCl} = 0.348) (Table 1) (Fig. 3b). At X_{KCl} > 0.348 the solubility of xenotime decreases to 122 ± 5 ppm (X_{KCl} = 0.493) (Fig. 3b). The data can be fit

using a second-degree polynomial function to describe the synthetic xenotime solubility as a function of X_{KCl} at 800°C and 1.0 GPa (Fig. 3b):

$$c_{xt} = -563\ X^2_{KCl} + 432\ X_{KCl} + 46 \quad (2)$$

where c_{xt} is the solubility of synthetic xenotime in ppm ($R^2 = 0.921$) and X_{KCl} is the mole fraction of KCl. Again xenotime solubilities are considerably higher in the system H_2O-NaCl as shown by Tropper et al. (2011) where the dissolved xenotime concentration increases with rising X_{NaCl} from 173 ppm (X_{NaCl} = 0.096) to 265 ppm (X_{NaCl} = 0.286) (Fig. 3b). At $X_{NaCl} > 0.286$ the solubility decreases to 212 ppm (X_{NaCl} = 0.399) and 191 ppm (X_{NaCl} = 0.496) (Fig. 3b). YPO_4 solubility in the system H_2O-NaCl by Tropper et al. (2011) increases in a manner similar to that of corundum and wollastonite (Newton and Manning, 2006), and shows a different trend than the solubility of YPO_4 in the system H_2O-KCl (Fig. 3b). Similar to the monazite-H_2O-KCl experiments, the xenotime-H_2O-KCl experiments have neutral quench pH values of 7 – 7.5 over the investigated X_{KCl} range (Table 1).

Figure 4 and Figure 5 show the relationship between the molality of xenotime vs. the mole fraction of KCl (X_{KCl}) and the activity of H_2O at 800°C and 1.0 GPa.

Discussion

Monazite and xenotime solubility as a function of X_{salt} at 800°C and 1.0 GPa

The low solubility of monazite and xenotime in pure H_2O experimentally obtained by Tropper et al. (2011) makes it difficult to explain the natural association of these minerals with metasomatic features in igneous and metamorphic rocks, such as hydrothermal alteration assemblages, veins, and skarns (e.g., Gieré, 1996). The fluid flux must be high enough to mobilize relatively insoluble REE, in which the solubility of (Y+REE) orthophosphates is low in near-neutral pH aqueous fluids and increases in acidic fluids (e.g. Tropper et al., 2013). An alternative mechanism for the dissolution and transportation of orthophosphate components is a high NaCl and/or KCl concentration in the fluid phase. Tropper et al. (2011) found that YPO_4 solubility in pure H_2O at 800°C and 1 GPa is greater (46 ppm) than that of $CePO_4$

(8 ppm). This is in nominal disagreement with the general observation that monazite is more common than xenotime in hydrothermal veins and other metasomatic features, which implies greater solubility of LREE relative to HREE and Y (e.g., Schmidt et al., 2007), and suggests that LREE are more abundant than HREE in such systems. However, REE and Y dissolution in natural fluids are controlled by ligands other than H_2O or phosphate, such as chloride, fluoride, and sulfate, all of which can be expected to occur in varying proportions (e.g., Williams-Jones et al., 2012). Consequently, experimental results obtained using pure H_2O only represent an end-member scenario unlikely to occur in nature.

To obtain information on the interaction of monazite and xenotime with pure H_2O and KCl + H_2O solutions, the following generalized dissolution reactions may be written (Newton and Manning, 2006, 2010; Tropper and Manning, 2011):

$$n\ CePO_4 + a\ KCl + b\ H_2O = k\ \text{solute species} \quad (3a)$$

or

$$n\ YPO_4 + a\ KCl + b\ H_2O = k\ \text{solute species} \quad (4a)$$

where n are the number of moles of monazite or xenotime, and a and b are the number of moles of KCl and H_2O consumed to produce k moles of solutes per mole of orthophosphate dissolved. The k moles of solutes per mole of orthophosphate were calculated assuming complete dissociation. The dissociation is represented by the following equations (Aranovich and Newton, 1996; Newton and Manning, 2006):

$$n\ Ce^{3+} + n\ PO_4^{3-} + a\ K^+ + a\ Cl^- + b\ H^+ + b\ OH^- = k \quad (3b)$$

or

$$n\ Y^{3+} + n\ PO_4^{3-} + a\ K^+ + a\ Cl^- + b\ H^+ + b\ OH^- = k \quad (4b)$$

The relative molar proportions of KCl and H_2O in Eqs. (3a) and (4a) were evaluated using the technique outlined in Newton and Manning (2006, 2010). In case that the solubility of monazite or xenotime decreases with X_{KCl}, then Ce^{3+} or Y^{3+} solutes would likely be hydrous species, and there would be no interaction with K^+ and/or Cl^-. Similarly, monotonic increase with X_{KCl} would imply no interaction with

299 H^+ and/or OH^-. If monazite and xenotime solubility increases to a plateau - like maximum and then
300 declines this would imply that their solutes include both hydrates and K- and/or Cl complexes. Figure 6a
301 and Figure 6b shows the variations in the relative solubility enhancements of synthetic monazite and
302 xenotime, expressed as a solute mole fraction for a given X_{KCl} relative to that in pure H_2O. The effect of
303 KCl on monazite and xenotime solubility can be assessed from the log-ratios $X_{mz} / X°_{mz}$ and $X_{xt} / X°_{xt}$,
304 where $X°_{mz}$ and $X°_{xt}$ are the mole fractions of monazite and xenotime in pure H_2O. The ratio log X/X°
305 thus represents the magnitude of solubility enhancement by a given KCl mole fraction.
306 Values of log X/X°, especially for synthetic monazite in KCl solutions, increase with increasing X_{KCl} over
307 the investigated range and this implies that the activity of H_2O does not significantly influence monazite
308 solubility (b = 0 in Eqn. 3a). This and the positive dependence of solubility on the square of X_{KCl} (Eqn. 1)
309 suggests that 3 moles of KCl per mole of $CePO_4$ form anhydrous solute species upon dissolution (a = 3).
310 A simple chemical equilibrium that could account for this relationship is:

311 $$1\ CePO_4 + 3\ KCl = 1\ CeCl_3 + 1\ K_3PO_4 \qquad (5)$$

312 The observed dissolution products in the KCl-bearing fluids are newly formed secondary monazite (Fig.
313 2a, Fig. 2b), $CeCl_3$, and K_3PO_4 (Eqn.5). Tropper et al. (2011) postulated that for the system monazite-
314 H_2O-NaCl a similar simple equilibrium could account for this relationship namely: $CePO_4 + 2NaCl =$
315 $CeCl_2^+ + Na_2PO_4^-$. Table 2a represents a chemical reaction model of the system monazite-H_2O-KCl, in
316 which the quantified reaction products of $CeCl_3$ and K_3PO_4 are listed.
317 In contrast to monazite, the values of log X/X° for the synthetic xenotime are not sufficiently precise to
318 define a maximum as in the NaCl system by Tropper et al. (2011). Nevertheless, the data rise with
319 increasing X_{KCl} over the investigated range to a maximum at X_{KCl} between 0.35 and 0.45 (Fig. 6b). This
320 implies that the activities of KCl and H_2O significantly influence xenotime solubility. Following the
321 approach of Newton and Manning (2006), the KCl mole fraction, at which the maximum solubility occurs,
322 defines the ratio of a to b in Eqn. 6 via:

$$X^{*}_{KCl} = \frac{a}{a+b} \quad (6)$$

and implies that a (for KCl) is 3 and b (for H_2O) varies between 5.5 (X_{KCl} = 0.35) and 3.6 (X_{KCl} = 0.45) (Fig. 6b). A simple chemical equilibrium that could account for this relationship at X_{KCl} = 0.43 is:

$$1\ YPO_4 + 4\ H_2O + 3\ KCl = 1\ YCl(OH)_2 + 1\ KH_2PO_4 + 2\ KOH + 2\ HCl \quad (7)$$

where a =3 and b = 4. The reaction products in the KCl-bearing fluids are $YCl(OH)_2$ (Fig. 1d, Fig. 2c), KH_2PO_4, KOH and HCl (Eqn. 7). The reverse reaction is defined as a neutralization reaction and occurs during the quenching process, in which the acid (HCl) and the base (KOH) react to form H_2O and KCl and the H^+ combines with OH^- to generate H_2O. This results in a quench pH equal to 7.

The dissolution products proposed in Eqs. (5) and (7) suggest that, in NaCl- and also KCl bearing fluids with neutral pH, the degree of Cl coordination for Y is lower than for Ce (Tropper et al., 2011). Assuming similar geochemical behavior for Y and REE, this is consistent with the steric hindrance of chloride complexation with HREE relative to LREE proposed by Mayanovic et al. (2009). The common occurrence of NaCl- and KCl-rich fluids in crustal and mantle settings (e.g., Newton et al., 1998; Yardley and Graham, 2002; Newton and Manning, 2010) could offer a simple mechanism to explain numerous cases of LREE mobility. Table 2b represents a chemical reaction model for the system xenotime-H_2O-KCl, in which the quantified reaction products of $YCl(OH)_2$ and KH_2PO_4 are listed.

Geological implications

Field studies of high-grade rocks show that the mobility of REE and Y in granulite-facies terranes is greatly enhanced in the presence of brines (e.g., Newton et al., 1998; Harlov, 2011; Aranovich et al., 2014) since brine-bearing fluid inclusions have been observed in granulites (e.g., Markl et al., 1998). It has therefore been proposed that REE (and by extension, Y) mobility may be enhanced by dissolved halogens in some cases as highly concentrated brines (e.g., Pan and Fleet, 1996; Schmidt et al., 2007; Antignano and Manning, 2008; Newton and Manning, 2010; Tropper et al., 2011, 2013). KCl brines or K-

rich fluids in the lower crust and upper mantle are, because of their high mechanical mobility and alkali-exchanging potential feasible metasomatic fluids for a variety of high grade rocks (Hansen et al., 1995; Newton et al., 1998; Harlov et al., 1998; Harlov and Förster, 2002a). Field observations (e.g., Touret and Nijland, 2013) and experimental investigations (Harlov, 2004) have demonstrated that a typical metasomatic feature associated with the presence of a high-salinity low-H_2O activity fluid is the presence of K-feldspar veining along the grain boundaries of minerals such as quartz, biotite, and plagioclase. Tropper et al. (2011) experimentally determined the solubility of $CePO_4$ monazite and YPO_4 xenotime in H_2O–NaCl solutions at 800 °C and 10 kbar. Their results indicate that the solubility of both Ce and Y increase with rising X_{NaCl}. Moreover, it has been shown that the most saline solutions exhibit a strong preference for LREE over HREE (Reed et al., 2000) and additional experiments in the system NaF-H_2O by Tropper et al. (2013) found that NaF solutions yielded an even stronger increase in Ce/Y concentration with rising salt concentrations. The present experiments in the system KCl-H_2O strongly corroborate the NaCl-H_2O experiments although the extent of solubility is lower. These experimental results help to explain key features of REE geochemistry in high-grade metamorphic processes since brine-induced anatexis will result in a noticeable depletion in the bulk REE concentration compared to parental rocks without the presence of brines as well as a decrease in the LREE/HREE ratio in the residual rock from which the melt was extracted.

Another important aspect is large-scale metasomatism involving brines. Metasomatic alteration is conjectured to involve infiltrating NaCl- and KCl-bearing brines during peak metamorphism as well as post peak and possibly more H_2O-rich fluids during uplift and cooling. Alkali-halide brines play an important role in mass transport (e.g. K-metasomatism) and mineral-fluid-melt phase equilibria in the lower crust (e.g., Newton et al., 1998; Yardley and Graham, 2002; Harlov and Förster, 2002a; Newton and Manning, 2010). With respect to the formation of large-scale ore deposits the experimental results by Harlov et al. (2002a), Taghipour et al. (2015) and Harlov et al. (2016) also support the extensive metasomatic alteration and remobilization of REE-enriched iron-oxide-apatite (IOA) deposits due to the

This is a preprint, the final version is subject to change, of the American Mineralogist (MSA)
Cite as Authors (Year) Title. American Mineralogist, in press.
(DOI will not work until issue is live.) DOI: http://dx.doi.org/10.2138/am-2017-6172

presence of brine-rich fluids. This fact is corroborated by a number of experiments, which have shown that the formation of monazite and xenotime associated with apatite is a metasomatically induced process that results from the interaction of brine-rich fluids that are reactive with the (Y + REE)-baring apatite (Harlov et al., 2002b; 2005; Harlov and Förster, 2003; Harlov, 2015; Harlov et al., 2016). These examples clearly show that further experimental investigations are still needed to understand the behavior of (Y+REE) carriers such as monazite and xenotime in the presence of brine-rich fluids, which frequently accompany high-grade metamorphism and metasomatic processes.

Acknowledgments

The financial support from the Institute of Mineralogy and Petrography, University of Innsbruck is greatly acknowledged. Martina Tribus is thanked for her help with the SEM and Hannes Witting for his help in the high-pressure laboratory. Craig E. Manning was supported by US National Science Foundation grant #EAR 1347987. The manuscript was significantly improved by reviews by Anselm Loges, and an anonymous reviewer. Don Baker is gratefully acknowledged for the editorial handling of the manuscript.

References cited

Agangi, A., Kamenetsky, V.S., and McPhie, J. (2010) The role of fluorine in the concentration and transportation of lithophile trace lements in felsic magmas: insights from the Gawler Range Volcanics, South Australia. Chemical Geology, 273, 314-325.

Ague, J.J. (1994a) Mass-transfer during Barrovian metamorphism of pelites, south-central Connecticut. 1. evidence for changes in composition and volume. American Journal of Science, 294, 1039-1057.

Ague, J.J. (1994b) Mass-transfer during Barrovian metamorphism of pelites, south-central Connecticut. 2. channelized fluid-flow and the growth of staurolite and kyanite. American Journal of Science, 294, 1061-1134.

Albino, G.V. (1995) Sodium metasomatism along the Melones Fault Zone, Sierra Nevada Foothills, California, USA. Mineralogical Magazine, 59, 383-400.

Antignano, A., and Manning, C.E. (2008) Fluorapatite solubility in H_2O and H_2O-NaCl at 700 to 900°C and 0.7 to 2.0 GPa. Chemical Geology, 251, 112-119.

Aranovich, L.Y., and Newton, R.C. (1996) H_2O activity in concentrated NaCl solutions at high pressures and temperatures measured by the brucite-periclase equilibrium. Contributions to Mineralogy and Petrology, 125, 200-212.

Aranovich, L.Y., and Newton, R.C. (1997) H_2O activity in concentrated KCI and KCI-NaC1 solutions at high temperatures and pressures measured by the brucite-periclase equilibrium. Contributions to Mineralogy and Petrology, 127, 261-271.

Aranovich, L.Y., and Newton, R.C. (1998) Reversed determination of the reaction: Phlogopite + quartz = enstatite + potassium feldspar + H_2O in the ranges 750-875 °C and 2-12 kbar at low H_2O activity with concentrated KCl solutions. American Mineralogist, 83, 193-204.

Aranovich, L.Y., Makhluf, A.R., Manning, C.E., and Newton, R.C. (2014) Dehydration melting

411 and the relationship between granites and granulites. Precambrian Research, 253, 26-37.
412 Barnes, J.D., Manning, C.E., Scambelluri, M., and Selverstone, J. (2017) The behavior of
413 halogens during subduction-zone processes. In Harlov, D., and Aranovich, L.Y., eds., The
414 Role of Halogens in Terrestrial and Extraterrestrial Geochemical Processes. Springer, in
415 press.
416 Billings, M.P. (1938) Introduction of potash during regional metamorphism in western New
417 Hampshire. Geological Society of America Bulletin, 49, 289-302.
418 Brennan, J. (1993) Partitioning of fluorine and chlorine between apatite and aqueous fluids at
419 high pressure and temperature: implications for the F and Cl content of high-P-T fluids.
420 Earth and Planetary Science Letters, 17, 251-263.
421 Caciagli, N.C., and Manning, C.E. (2003) The solubility of calcite in water at 6–16 kbar and 500–
422 800 degrees C. Contributions to Mineralogy and Petrology, 146, 275-285.
423 Cherniak, D.J., Pyle, J., and Rakovan, J. (2004) Synthesis of REE and Y phosphates by Pb-free
424 flux methods and their utilization as standards for electron microprobe analysis and in
425 design of monazite chemical U–Th–Pb dating protocol. American Mineralogist, 89, 1533-
426 1539.
427 DeJong, G., and Williams, P.J. (1995) Giant metasomatic system formed during exhumation of
428 mid-crustal Proterozoic rocks in the vicinity of the Cloncurry Fault, northern Queensland.
429 Australian Journal of Earth Sciences, 42, 281-290.
430 Dunbar, N.W., Campbell, A.R., and Candela, P.A. (1996) Physical, chemical, and mineralogical
431 evidence for magmatic fluid migration within the Capitan pluton, southeastern New
432 Mexico. Geological Society of America Bulletin, 108, 318-333.
433 Ewing, R. (2001) The design and evaluation of nuclear-wasteforms: clues from mineralogy. The
434 Canadian Mineralogist, 39, 697-715.

435 Gao, J., John, T., Klemd, R., and Xiong X. (2007) Mobilization of Ti-Nb-Ta during subduction:
436 Evidence from rutile-bearing dehydration segregations and veins hosted in eclogite,
437 Tianshan, NW China. Geochimica et Cosmochimica Acta, 71, 4974-4996.
438 Gieré, R. (1996) Formation of rare earth minerals in hydrothermal systems. In: Jones, A.P., Wall,
439 F., Williams, C.T. (Eds.), Rare Earth Minerals. Chapman and Hall, 105-150.
440 Gratz, R., and Heinrich, W. (1997) Monazite-xenotime thermobarometry: Experimental
441 calibration of the miscibility gap in the binary system $CePO_4$-YPO_4. American
442 Mineralogist, 82, 772-780.
443 Hansen, E.C., Newton, R.C., Janardhan, A.S., and Lindenberg, S. (1995) Differentiation of late
444 Archean crust in the eastern Dharwar Craton, Krishnagiri-Salem Area, South India.
445 Journal of Geology, 103, 629-651.
446 Harlov, D.E. (2004) Fluid Induced Dehydration of the Mafic Lower Crust from Amphibolite to
447 Granulite Facies: Nature and Experiment. American Geophysical Union, Fall Meeting
448 2004, abstract #V31A-1409.
449 Harlov, D. (2011) Petrological and experimental application of REE- and actinide-bearing
450 accessory minerals to the study of Precambrian high-grade gneiss terranes. Special Paper
451 Geological Society of America Memoirs: Origin and Evolution of Precambrian High-
452 Grade Gneiss Terrains, with Special Emphasis on the Limpopo Complex of Southern
453 Africa pp. 13-24.
454 Harlov, D.E. (2012) The potential role of fluids during regional granulite-facies dehydration in
455 the lower crust. Geoscience Frontiers, 3, 813-827.
456 Harlov, D.E. (2015) Apatite and fluids: A fingerprint for metasomatic processes. Elements, 11,
457 171-176.

458 Harlov, D.E., Hansen, E.C., and Bigler, C. (1998) Petrologic evidence for K-feldspar
459 metasomatism in granulite facies rocks. Chemical Geology, 151, 373-386.
460 Harlov, D.E., and Förster, H-J. (2002a) High-grade fluid metasomatism on both local and a
461 regional scale: the Seward Peninsula, Alaska, and the Val Strona Omegna, Ivrea-Verbano
462 Zone, Northern Italy. Part II: phosphate mineral chemistry. Journal of Petrology, 43, 801-
463 824.
464 Harlov, D.E., Förster, H.-J. and Nijland, T.G. (2002b) Fluid-induced nucleation of REE-
465 phosphate minerals in fluorapatite: Nature and experiment Part I. Chlorapatite. American
466 Mineralogist, 87, 245-261.
467 Harlov, D.E., and Förster, H.-J. (2003) Fluid-induced nucleation of (Y + REE)-phosphate
468 minerals within fluorapatite: Nature and experiment. Part II. Fluorapatite: American
469 Mineralogist, 88, 1209-1229.
470 Harlov, D.E., Wirth, R., and Förster, H.-J. (2005) An experimental study of dissolution-
471 reprecipitation in fluorapatite: fluid infiltration and the formation of monazite.
472 Contributions to Mineralogy and Petrology, 150, 268-286.
473 Harlov, D., Tropper, P., Seifert, W., Nijland, T., and Förster, H.-J. (2006) Formation of Al-rich
474 titanite ($CaTiSiO_4O$-$CaAlSiO_4OH$) reaction rims on ilmenite in metamorphic rocks as a
475 function of fH_2O and fO_2. Lithos, 88, 72-84.
476 Harlov, D.E., Meighan, C.J., Kerr, I.D., and Samson, I.M. (2016) Mineralogy, chemistry, and
477 fluid-aided evolution of the Pea Ridge Fe oxide-(Y+REE) deposit, southeast Missouri,
478 USA. Economic Geology, 111, 1963-1984.
479 Harlow, G.E., and Davies, R. (2004) Status report on stability of K-rich phases at mantle
480 conditions. Lithos, 77, 647-653.

Harrison, T.M., Catlos, E., and Montel, J.M. (2002) U-Th-Pb dating of phosphate minerals. Reviews in Mineralogy and Geochemistry, 48, 523-577.

Haschke, J.M. (1974) Structural Relationships, Crystal Chemistry and Anion Substitution Processes for $M(III)X_3$ Systems of the Lanthanides and Actinides. Journal of Solid State Chemistry, 14, 238-246.

Ionov, D.A., and Hofmann, A.W. (1995) Nb-Ta-rich mantle amphiboles and micas: Implications for subduction-related metasomatic trace element fractionations. Earth and Planetary Science Letters, 131, 341-356.

Janots, E., Engi, M., Berger, A., Allaz, J., Schwarz, J.-O., and Spandler, C. (2008) Prograde metamorphic sequence of REE minerals in pelitic rocks of the Central Alps: implications for allanite-monazite-xenotime phase relations from 250 to 610 °C. Journal of Metamorphic Geology, 26, 509-526.

Janots, E., Engi, M., Rubatto, D., Berger, A., Gregory, C., and Rahn, M. (2009) Metamorphic rates in collisional orogeny from in situ allanite and monazite dating. Geology, 37, 11-14.

Kamenetsky, M.B., Sobolev, A.V., Kamenetsky, V.S., Maas, R., Danyushevsky, L.V., Thomas, R., Pokhilenko, N.P., and Sobolev, N.V. (2004) Kimberlite melts rich in alkali chlorides and carbonates; a potent metasomatic agent in the mantle. Geology, 32, 845-848.

Keppler, H. (2017) Fluids and trace element transport in subduction zones. American Mineralogist, 102, 5-20.

Klevtsova, R.F., and Klevtsov, P.V. (1965) Growth Forms and Crystal Structure of $YCl(OH)_2$. Soviet Physics Doklady, 10, 487.

Manning, C.E. (2004) The chemistry of subduction-zone fluids. Earth and Planetary Science Letters, 223, 1-16.

Markl, G., Ferry, J.M., and Bucher, K. (1998) Formation of saline brines and salt in the lower

505 crust by hydration reactions in partially retrogressed granulites from the Lofoten Islands,
506 Norway. American Journal of Science, 298, 705-57.
507 Markl, G., and Piazolo, S. (1998) Halogen-bearing minerals in syenites and high-grade marbles
508 of Dronning Maud Land, Antarctica: monitors of fluid compositional changes during late-
509 magmatic fluid-rock interaction processes. Contributions to Mineralogy and Petrology,
510 132, 246-268.
511 Mayanovic, R.A., Anderson, A.J., Basset, W.A., and Chou, I.M. (2009) Steric hindrance and the
512 enhanced stability of light rare-earth elements in hydrothermal fluids. American
513 Mineralogist, 94, 1487-1490.
514 Montel, J.M. (1993) A model for monazite/melt equilibrium and application to the generation of
515 granitic magmas. Chemical Geology, 110, 127-146.
516 Newton, R.C., Aranovich, L.Y., Hansen, E.C., and Vandenheuvel, B.A. (1998) Hypersaline
517 fluids in Precambrian deep-crustal metamorphism. Precambrian Research, 91, 41-63.
518 Newton, R.C., and Manning, C.E. (2002) Experimental determination of calcite solubility in
519 H_2O-NaCl solutions at deep crust/upper mantle pressures and temperatures: implications
520 for metasomatic processes in shear zones. American Mineralogist, 87, 1401-1409.
521 Newton, R.C., and Manning, C.E. (2005) Solubility of anhydrite, $CaSO_4$, in NaCl-H_2O solutions
522 at high pressures and temperatures: applications to fluid-rock interaction. Journal of
523 Petrology, 46, 701-716.
524 Newton R.C., and Manning C.E. (2006) Solubilities of corundum, wollastonite and quartz in
525 H_2O-NaCl solutions at 800°C and 10 kbar: Interaction of simple minerals with brines at
526 high pressure and temperature. Geochimica et Cosmochimica Acta, 70, 5571-82.
527 Newton R.C., and Manning C.E. (2010) Role of saline fluids in deep-crustal and upper-mantle
528 metasomatism: insights from experimental studies. Geofluids, 10, 58-72.

529 Pan, Y., Fleet, M.E. (1996) Rare element mobility during prograde granulite facies
530 metamorphism: significance of fluorine. Contributions to Mineralogy and Petrology, 123,
531 251-262.
532 Pasteris, J.D., Harris, T.N., and Sassari, D.C. (1995) Interactions of mixed volatile-brine fluids in
533 rocks of the southwestern footwall of the Duluth Complex, Minnesota – evidence from
534 aqueous fluid inclusions. American Journal of Science, 295, 125-172.
535 Philippot, P., Chevallier, P., Chopin, C., and Dubessy, J. (1995) Fluid composition and evolution
536 in coesite-bearing rocks (Dora Maira massif, western Alpa): implications for element
537 recycling during subduction. Contributions to Mineralogy and Petrology, 121, 29-41.
538 Philippot, P., and Selverstone, J. (1991) Trace element-rich brines in eclogitic veins: implications
539 for fluid compositions and transport during subduction. Contributions to Mineralogy and
540 Petrology, 106, 417-430.
541 Reed, M.J., Candela, P.A., and Piccoli, P.M. (2000) The distribution of rare earth elements
542 between monzogranitic melt and the aqueous volatile phase in experimental investigations
543 at 800 °C and 200 MPa. Contributions to Mineralogy and Petrology, 140, 251-262.
544 Rubatto, D., and Hermann, J. (2003) Zircon formation during fluid circulation in eclogites
545 (Monviso, Western Alps): implications for Zr and Hf budget in subduction zones.
546 Geochimica et Cosmochimica Acta, 67, 2173-2187.
547 Safonov, O.G., Kovaleva, E.I., Kosova, S.A., Rajesh, H.M., Belyanin, G.A., Golunova, M.A.,
548 and Van Reenen, D.D. (2012) Experimental and petrological constraints on local-scale
549 interaction of biotite-amphibole gneiss with H_2O-CO_2-(K, Na)Cl fluids at middle-crustal
550 conditions: Example from the Limpopo Complex, South Africa. Geoscience Frontiers, 3,
551 829-841.

552 Sampson, I.M., Liu, W., and Williams-Jones, A.E. (1995) The nature of orthomagmatic fluids in
553 the Oka carbonatite, Quebec, Canada: evidence from fluid inclusions. Geochimica et
554 Cosmochimica Acta, 59, 1963-1977.
555 Schmidt, C., Rickers, K., Bilderback, D.H., and Huang, R. (2007) In situ synchrotron radiation
556 XRF study of REE phosphate dissolution in aqueous fluids to 800°C. Lithos, 95, 87-102.
557 Shmulovich, K.I., Yardley, B.W.D., and Graham, C.M. (2005) The solubility of quartz in
558 chloride solutions at 400°-800°C and 0.1-0.9 GPa. Goldschmidt Conference Abstract
559 2005, abstract #V69A-823.
560 Spear, F.S., and Pyle, J.M. (2002) Apatite, monazite and xenotime in metamorphic rocks.
561 Reviews in Mineralogy and Geochemistry, 48, 293-335.
562 Taghipour, S., Kananian, A., Harlov, D., and Oberhänsli, R. (2015) Kiruna-type iron oxide-
563 apatite deposits, Bafq district, central Iran: fluid-aided genesis of fluorapatite-monazite-
564 xenotime assemblages. The Canadian Mineralogist, 53, 479-496.
565 Todd, C.S., and Evans B.W. (1994) Properties of CO_2-induced dehydration of amphibolite.
566 Journal of Petrology, 35, 1213-1240.
567 Tomlinson, E., Jones, A., and Milledge, J. (2004) High-pressure experimental growth of diamond
568 using C–K_2CO_3–KCl as an analogue for Cl-bearing carbonate fluid. Lithos, 77, 287-294.
569 Touret, J.L.R. (1985) Fluid regime in southern Norway: the record of fluid inclusions. Tobi AC,
570 Touret JRL (eds) The deep Proterozoic crust in the North Atlantic provinces. Reidel,
571 Dordrecht pp 517-549.
572 Touret, J.L.R., and Nijland, T.G. (2013) Metasomatism and the Chemical Transformation of
573 Rock. The Role of Fluids in Terrestrial and Extraterrestrial Processes. Part of the series
574 Lecture Notes in Earth System Sciences pp 415-469. Springer Berlin, Heidelberg.

575 Tropper, P., and Manning, C.E. (2005) Very low solubility of rutile in H_2O at high pressure and
576 temperature, and its implications for Ti-mobility in subduction zones. American
577 Mineralogist, 90, 502-505.
578 Tropper, P., and Manning, C.E. (2007a) The solubility of fluorite in H_2O and H_2O-NaCl at high
579 pressure and temperature. Chemical Geology, 242, 299-306.
580 Tropper, P., and Manning, C.E. (2007b) The solubility of corundum in H_2O at high pressure and
581 temperature and its implications for Al mobility in the deep crust and upper mantle.
582 Chemical Geology, 240, 54-60.
583 Tropper, P., Manning, C.E., and Harlov, D.E. (2011) Solubility of $CePO_4$ monazite and YPO_4
584 xenotime in H_2O and H_2O-NaCl at 800°C and 1 GPa: implications for REE and Y
585 transport during high-grade metamorphism. Chemical Geology, 282, 58-66.
586 Tropper, P., Manning, C.E., and Harlov, D.E. (2013) Solubility of $CePO_4$ monazite and YPO_4
587 xenotime in H_2O-NaF at 800°C and 1 GPa. Geofluids, 13, 372-380.
588 Williams-Jones, A.E., Migdisov, A.A., and Samson, I.M. (2012) Hydrothermal mobilization of
589 the REE – a tale of ceria and yttria. Elements, 8, 355-360.
590 Yang, X.-M., Yang, X.-Y., Zheng, Y.-F., and Le Bas, M.J. (2003) A rare earth element-rich
591 carbonatite dyke at Bayan Obo, Inner Mongolia, North China. Mineralogy and Petrology,
592 78, 93-110.
593 Yardley, B.W.D. (1985) Apatite composition and the fugacities of HF and HCl in metamorphic
594 fluids. Mineralogical Magazine, 49, 77-79.
595 Yardley, B.W.D., and Graham, J.T. (2002) The origins of salinity in metamorphic fluids
596 Geofluids, 2, 249-256.
597 Zhuravleva, M., Stand, L., Wei, H., Hobbs, C., Boatner, L.A., Ramey, J.O., Shah, K., Burger, A.,
598 Rowe, E., Bhattacharya, P., Tupitsyn, E., and Melcher, C.L. (2013) Hygroscopicity

599 evaluation of halide scintillators. Nuclear Science Symposium and Medical Imaging
600 Conference (NSS/MIC), 2013 IEEE.

601

602

603

This is a preprint, the final version is subject to change, of the American Mineralogist (MSA)
Cite as Authors (Year) Title. American Mineralogist, in press.
(DOI will not work until issue is live.) DOI: http://dx.doi.org/10.2138/am-2017-6172

Figure captions

Figure 1. SEM images of run products from selected experiments. (a) $CePO_4$ crystal after dissolution at $X_{KCl} = 0.101$ (Mnz_003). (b) Surface of the $CePO_4$ crystal dissolved in $X_{KCl} = 0.101$, displaying dissolution grooves and recrystallization. (c) YPO_4 crystal after dissoultion at $X_{KCl} = 0.348$ (Xnt_028). (d) YPO_4 crystal after dissolution in $X_{KCl} = 0.099$ (Xnt_023) fluid, with tiny quench crystals ($YCl(OH)_2$) adhering to the surface.

Figure 2. SEM images of the quench material from selected experiments. (a,b) Two generations of secondary monazite crystals, that occur as prismatic needles (sec mz I) and stellate clusters (sec mz II), which nucleated in the outer casule upon quench and embedded in KCl aggregates. (c,d) Tabular – prismatic crystal of $YCl(OH)_2$ and secondary xenotime crystals (sec xt), which embedded in KCl aggregates.

Figure 3a. Monazite solubility versus the mole fraction of KCl and NaCl (X_i) at 800°C and 1.0 GPa. The error bars are 2σ and are calculated based on the weighing uncertainties. The solid line in the system monazite-KCl-H_2O represents the fitted solubilities from Eqn. (1). Results of Tropper et al. (2011) from monazite-NaCl-H_2O at 800°C and 1.0 GPa shown for comparison. Halite- and sylvite saturation estimated from Aranovich and Newton (1996, 1997).

Figure 3b. Xenotime solubility versus the mole fraction of KCl and NaCl (X_i) at 800°C and 1.0 GPa. The error bars are 2σ and are calculated based on the weighing uncertainties. The solid line in the system xenotime-KCl-H_2O represents the fitted solubilities from Eqn. (2). Results of Tropper et al. (2011) from xenotime-NaCl-H_2O at 800°C and 1.0 GPa shown for comparison. Halite- and sylvite saturation estimated from Aranovich and Newton (1996, 1997).

This is a preprint, the final version is subject to change, of the American Mineralogist (MSA)
Cite as Authors (Year) Title. American Mineralogist, in press.
(DOI will not work until issue is live.) DOI: http://dx.doi.org/10.2138/am-2017-6172

Figure 4. The relation between the molality of monazite and xenotime vs. the mole fraction of KCl and NaCl (X_i) at 800°C and 1.0 GPa. Results of Tropper et al. (2011) from monazite and xenotime in the system NaCl-H_2O at 800°C and 1.0 GPa are shown for comparison. Halite- and sylvite saturation estimated from Aranovich and Newton (1996, 1997).

Figure 5. The relation between the molality of monazite and xenotime in the system H_2O-KCl vs. the activity of H_2O at 800°C and 1.0 GPa.

Figure 6a. Logarithm of the solubility enhancement of monazite, $X_{mz}/X°_{mz}$, versus X_{KCl} at 800°C and 1.0 GPa. Values of log $X_{mz}/X°_{mz}$ increase continuously with increasing X_{KCl} over the investigated range and this implies that the activity of H_2O does not significantly influence monazite solubility (b=0). This suggests that 3 moles of KCl per mole of $CePO_4$ form anhydrous solute species upon dissolution (a=3).

Figure 6b. Logarithm of the solubility enhancement of xenotime, $X_{xt}/X°_{xt}$, versus X_{KCl} at 800°C and 1.0 GPa. Values of $X_{xt}/X°_{xt}$ rise with increasing X_{KCl} over the investigated range to a maximum at X_{KCl} between 0.35 and 0.45. This implies that the activities of KCl and H_2O significantly influence xenotime solubility and that a (for KCl) is 3 and b (for H_2O) varies between 5.5 (X_{KCl} = 0.35) and 3.6 (X_{KCl} = 0.45).

644 # Tables

645 **Table 1:** Experimental results in the system Monazite-H_2O-KCl and Xenotime-H_2O-KCl at
646 800°C and 1.0 GPa

Run number	Time (h)	H_2O in (mg)	KCl in (mg)	X_{KCl}	Crystal in (mg)	Crystal out (mg)	Solubility (ppm)	pH
Synthetic Monazite - H_2O - KCl								
Mnz-18*	90	35.89	0.00	0.000	1.1635	1.1632	8	-
Mnz_003	12	35.20	16.44	0.101	2.8190	2.8150	78 (4)	7.0
Mnz_005	12	31.01	23.11	0.153	2.6666	2.6603	116 (2)	7.0
Mnz_013	12	21.77	31.44	0.259	1.3995	1.3872	232 (6)	7.5
Mnz_012	12	14.08	38.07	0.395	1.6765	1.6615	288 (8)	7.0
Mnz_015	12	9.08	38.50	0.506	1.0983	1.0823	335 (3)	7.5
Natural Monazite - H_2O - KCl								
Mnz_017	12	21.31	31.38	0.262	1.2343	1.2245	186 (3)	8.0
Synthetic Xenotime - H_2O - KCl								
Xnt-4*	12	41.62	0.00	0.000	2.3541	2.3522	46	-
Xnt_023	12	34.60	15.81	0.099	0.8727	0.8693	67 (5)	7.0
Xnt_024	12	25.59	27.31	0.205	0.9871	0.9805	124 (1)	7.5
Xnt_028	12	16.31	36.07	0.348	0.9329	0.9263	126 (4)	7.5
Xnt_027	12	10.47	42.17	0.493	0.7068	0.7004	122 (5)	7.5

647

648 Explanation: "Crystal in" and "Crystal out" refer respectively to the weights before and after the experiment. Weights reported to two decimal
649 places were determined on a Mettler Toledo AX205 DeltaRange microbalance ($1\sigma = 0.03$ mg); those to four places were determined on a Mettler
650 Toledo XP2U ultra microbalance ($1\sigma = 0.1$ µg). The solubility is expressed with the 1σ uncertainty, based on propagation of weighing errors. Run
651 numbers Mnz-18 and Xnt-4, which are marked with a star, are the experiments in pure H_2O at 800°C and 1.0 GPa from Tropper et al. (2011).

652

This is a preprint, the final version is subject to change, of the American Mineralogist (MSA)
Cite as Authors (Year) Title. American Mineralogist, in press.
(DOI will not work until issue is live.) DOI: http://dx.doi.org/10.2138/am-2017-6172

Table 2a: Chemical reaction model of the system monazite-H_2O-KCl. Based on the limiting reactant approach for monazite, the dissolution reaction 1 $CePO_4$ + 3 KCl = 1 $CeCl_3$ + 1 K_3PO_4 occurs over the investigated range of X_{KCl} (0.101 – 0.506) and implies no interaction with H_2O. The amount of water remains unchanged before and after the chemical reaction (m H_2O = m H_2O rest)

Monazite - KCl **1** $CePO_4$ + **3** KCl =					**1** $CeCl_3$ + **1** K_3PO_4				
Run number	Δm $CePO_4$ [µg]	m H_2O [mg]	m KCl [mg]	X_{KCl}	m $CeCl_3$ [µg]	m K_3PO_4 [µg]	m H_2O rest [mg]	m KCl rest [mg]	obs pH
Mnz_003	4.05	35.20	16.440	**0.101**	4.25	3.66	35.20	16.436	7.0
Run number	Δm $CePO_4$ [µg]	m H_2O [mg]	m KCl [mg]	X_{KCl}	m $CeCl_3$ [µg]	m K_3PO_4 [µg]	m H_2O rest [mg]	m KCl rest [mg]	obs pH
Mnz_013	12.35	21.77	31.440	**0.259**	12.95	11.15	21.77	31.428	7.5
Run number	Δm $CePO_4$ [µg]	m H_2O [mg]	m KCl [mg]	X_{KCl}	m $CeCl_3$ [µg]	m K_3PO_4 [µg]	m H_2O rest [mg]	m KCl rest [mg]	obs pH
Mnz_015	15.98	9.08	38.503	**0.506**	16.75	14.42	9.08	38.487	7.5

Table 2b: Chemical reaction model of the system xenotime-H_2O-KCl. Based on the limiting reactant approach for xenotime, the dissolution reaction 1 YPO_4 + 4 H_2O + 3 KCl = 1 $YCl(OH)_2$ + 1 KH_2PO_4 + 2 HCl + 2 KOH occurs over the investigated range of X_{KCl} (0.35 – 0.45) and implies an interaction with KCl and H_2O. The corresponding amounts of water and salt change accordingly after the chemical reaction (m H_2O > m H_2O rest and m KCl > m KCl rest)

Xenotime - H_2O - KCl **1** YPO_4 + **4** H_2O + **3** KCl =					**1** $YCl(OH)_2$ + **1** KH_2PO_4 + **2** HCl + **2** KOH						
Run number	Δm YPO_4 [µg]	m H_2O [mg]	m KCl [mg]	X_{KCl}	m $YCl(OH)_2$ [µg]	m KH_2PO_4 [µg]	m HCl [µg]	m (KOH) [µg]	m H_2O rest [mg]	m KCl rest [mg]	obs pH
Xnt_028	6.60	16.310	36.070	**0.348**	5.68	4.88	2.62	4.03	16.307	36.062	7.5
Run number	Δm YPO_4 [µg]	m H_2O [mg]	m KCl [mg]	X_{KCl}	m $YCl(OH)_2$ [µg]	m KH_2PO_4 [µg]	m HCl [µg]	m (KOH) [µg]	m H_2O rest [mg]	m KCl rest [mg]	obs pH
Xnt_027	6.40	10.468	35.500	**0.493**	5.51	4.74	2.54	3.91	10.465	35.492	7.5

This is a preprint, the final version is subject to change, of the American Mineralogist (MSA)
Cite as Authors (Year) Title. American Mineralogist, in press.
(DOI will not work until issue is live.) DOI: http://dx.doi.org/10.2138/am-2017-6172

667 **Figures**

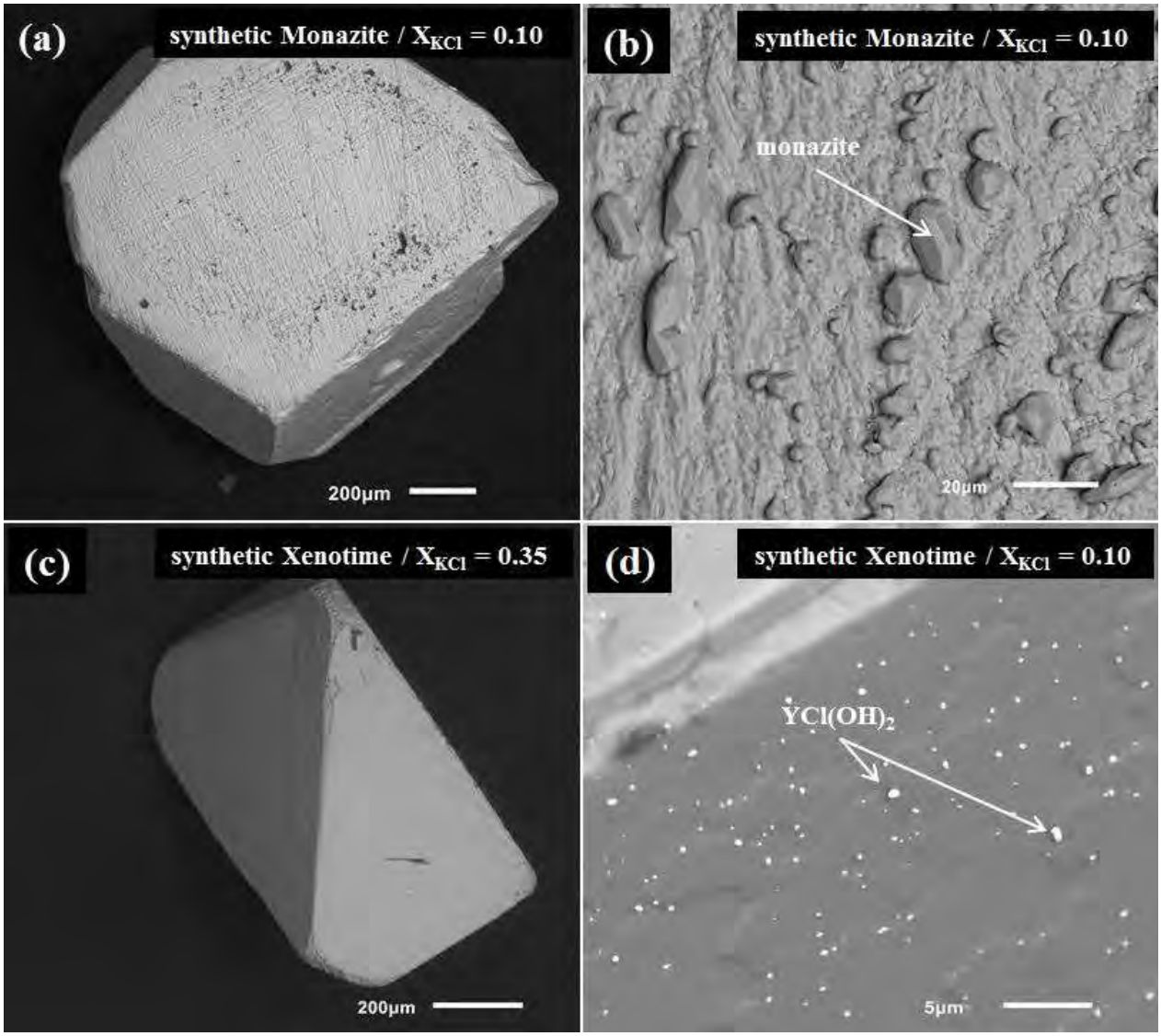

668 **Figure 1.**

669

This is a preprint, the final version is subject to change, of the American Mineralogist (MSA)
Cite as Authors (Year) Title. American Mineralogist, in press.
(DOI will not work until issue is live.) DOI: http://dx.doi.org/10.2138/am-2017-6172

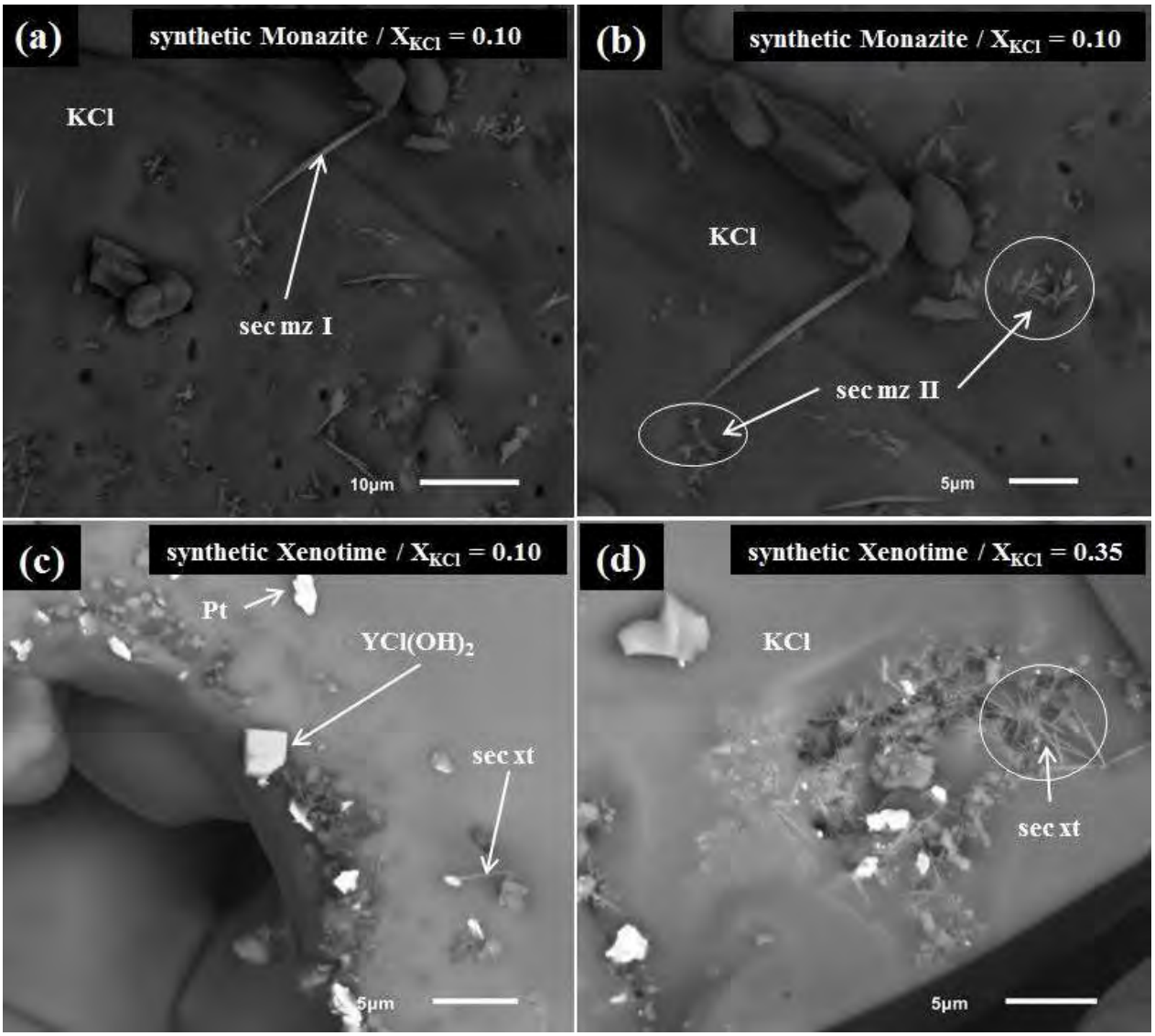

Figure 2.

This is a preprint, the final version is subject to change, of the American Mineralogist (MSA)
Cite as Authors (Year) Title. American Mineralogist, in press.
(DOI will not work until issue is live.) DOI: http://dx.doi.org/10.2138/am-2017-6172

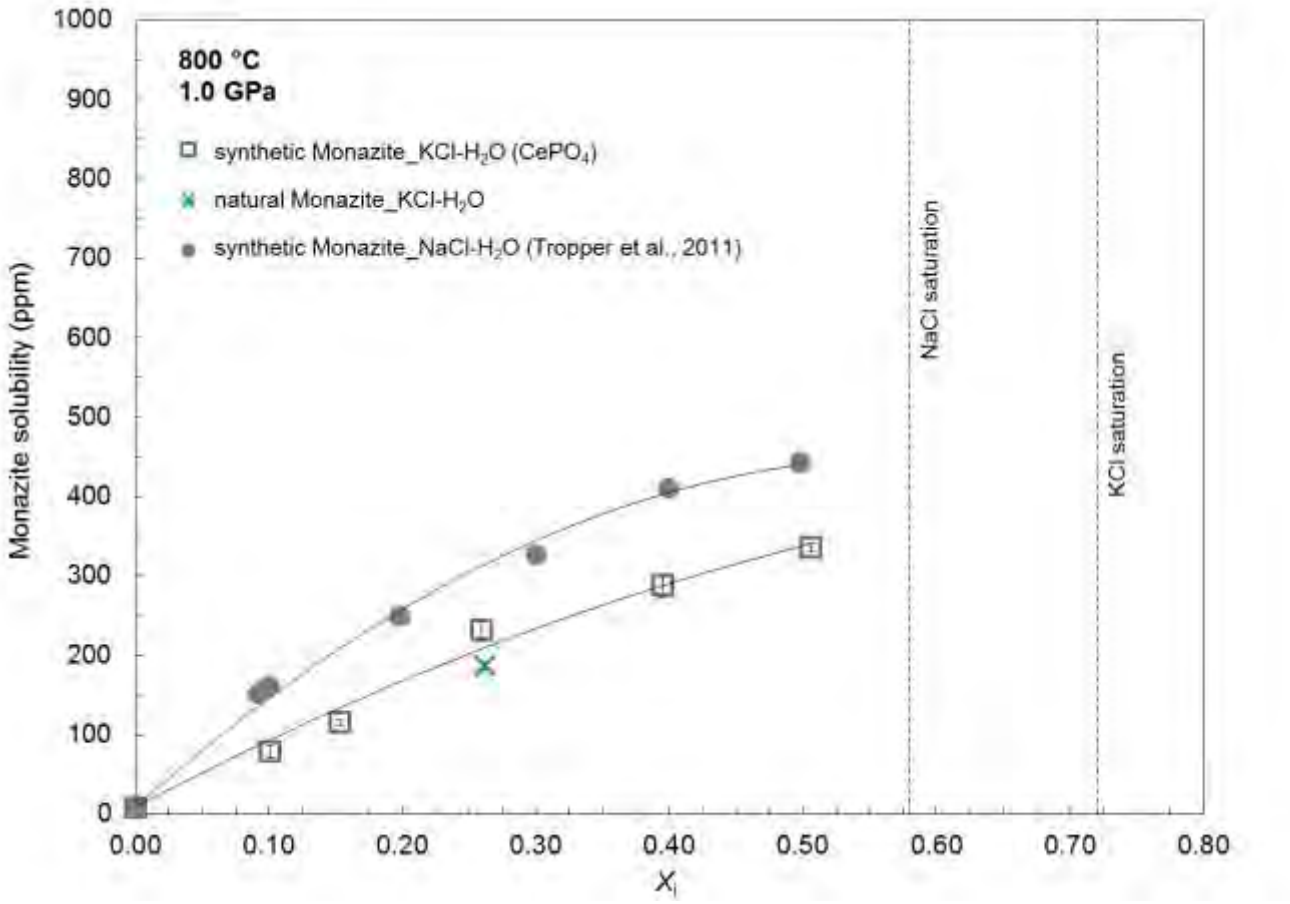

675

676 **Figure 3a.**

677

This is a preprint, the final version is subject to change, of the American Mineralogist (MSA)
Cite as Authors (Year) Title. American Mineralogist, in press.
(DOI will not work until issue is live.) DOI: http://dx.doi.org/10.2138/am-2017-6172

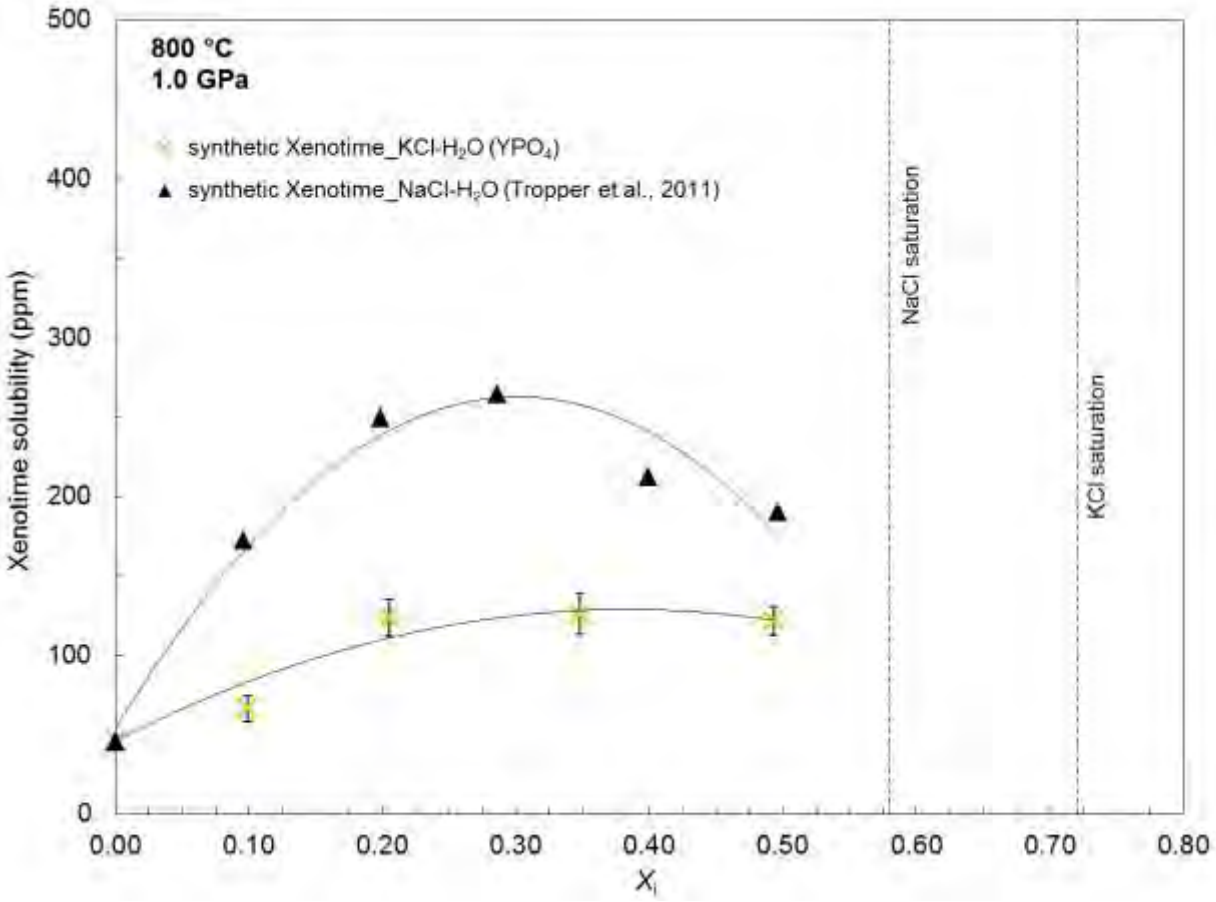

Figure 3b.

This is a preprint, the final version is subject to change, of the American Mineralogist (MSA)
Cite as Authors (Year) Title. American Mineralogist, in press.
(DOI will not work until issue is live.) DOI: http://dx.doi.org/10.2138/am-2017-6172

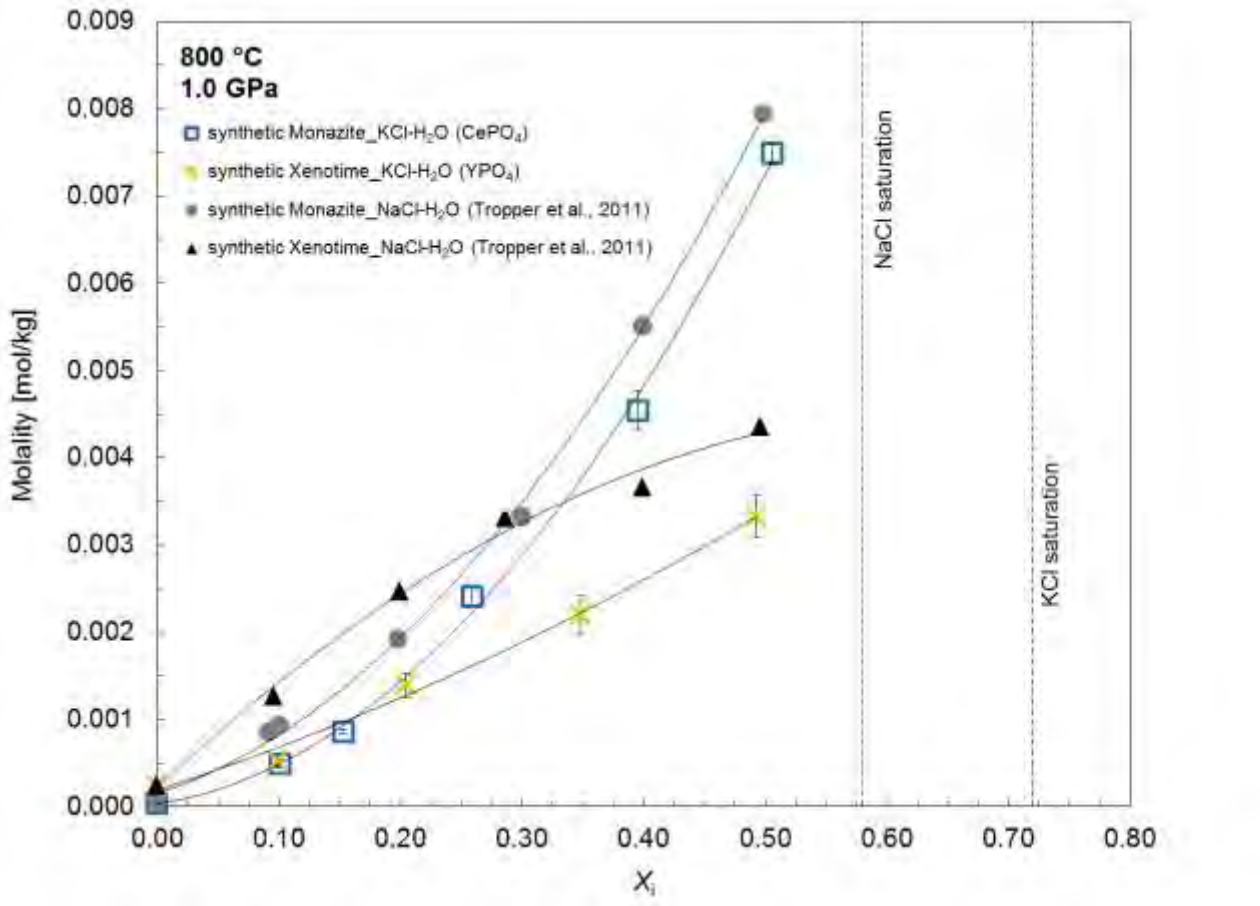

Figure 4.

This is a preprint, the final version is subject to change, of the American Mineralogist (MSA)
Cite as Authors (Year) Title. American Mineralogist, in press.
(DOI will not work until issue is live.) DOI: http://dx.doi.org/10.2138/am-2017-6172

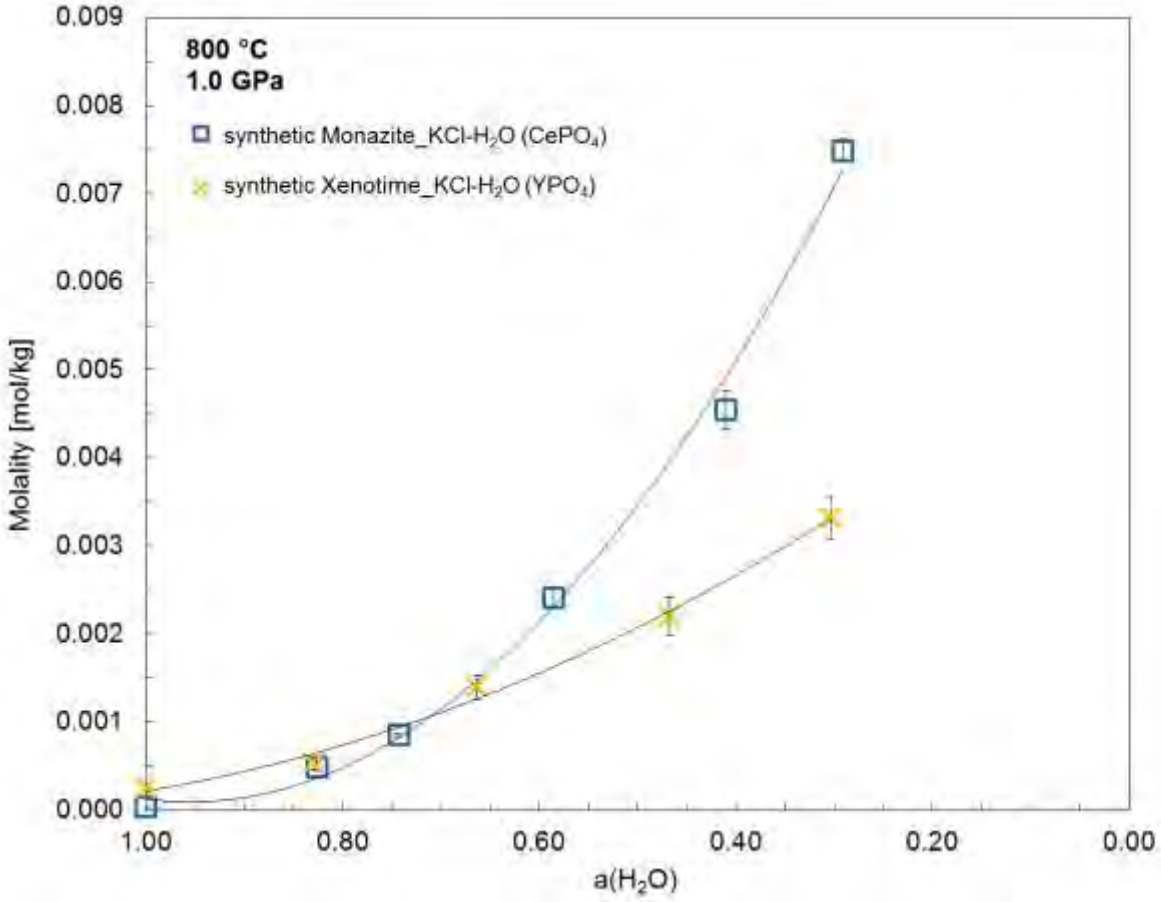

690

691 **Figure 5.**

692

693

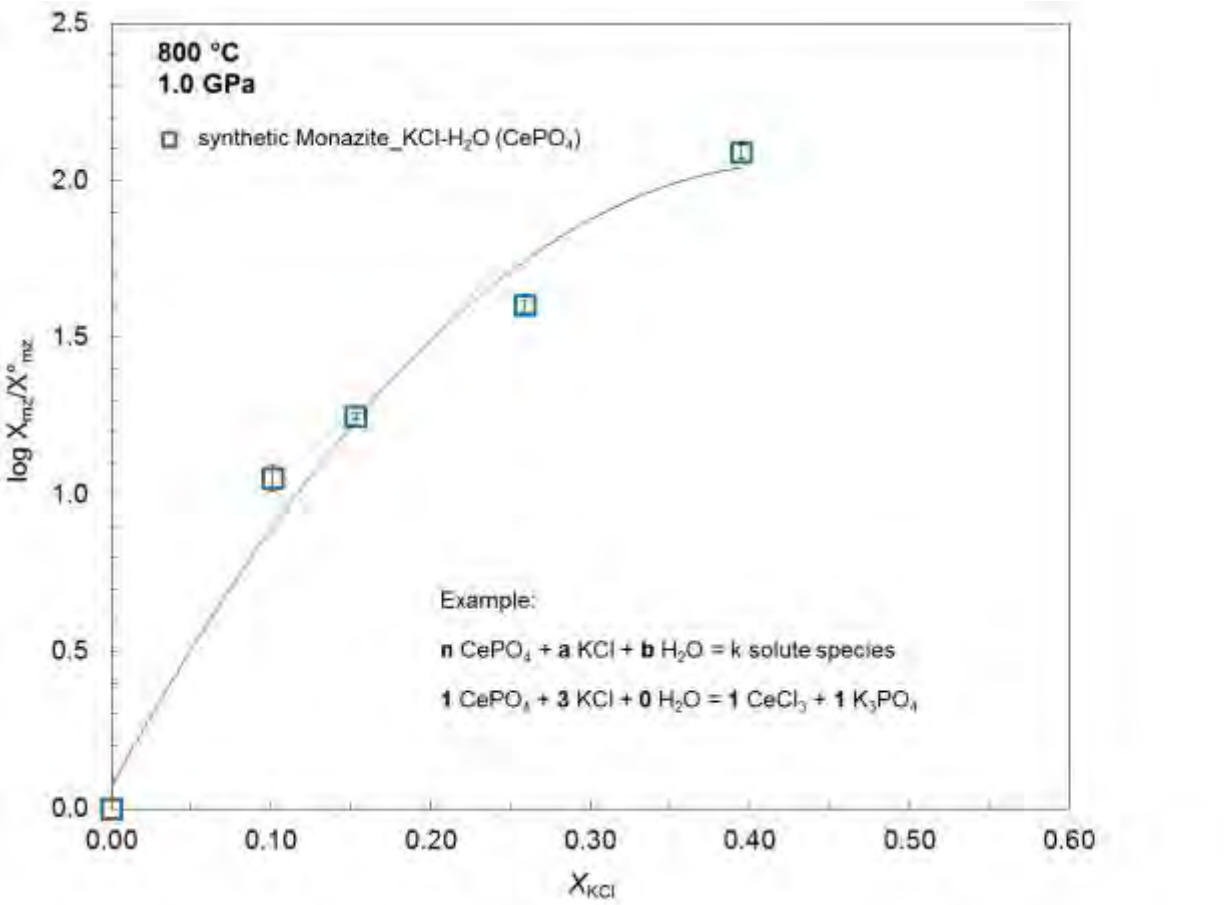
800 °C
1.0 GPa
synthetic Monazite_KCl-H2O (CePO4)
log Xmz/X°mz
XKCl
Example:
n CePO4 + a KCl + b H2O = k solute species
1 CePO4 + 3 KCl + 0 H2O = 1 CeCl3 + 1 K3PO4
0.0
0.5
1.0
1.5
2.0
2.5
0.00
0.10
0.20
0.30
0.40
0.50
0.60

Figure 6a.

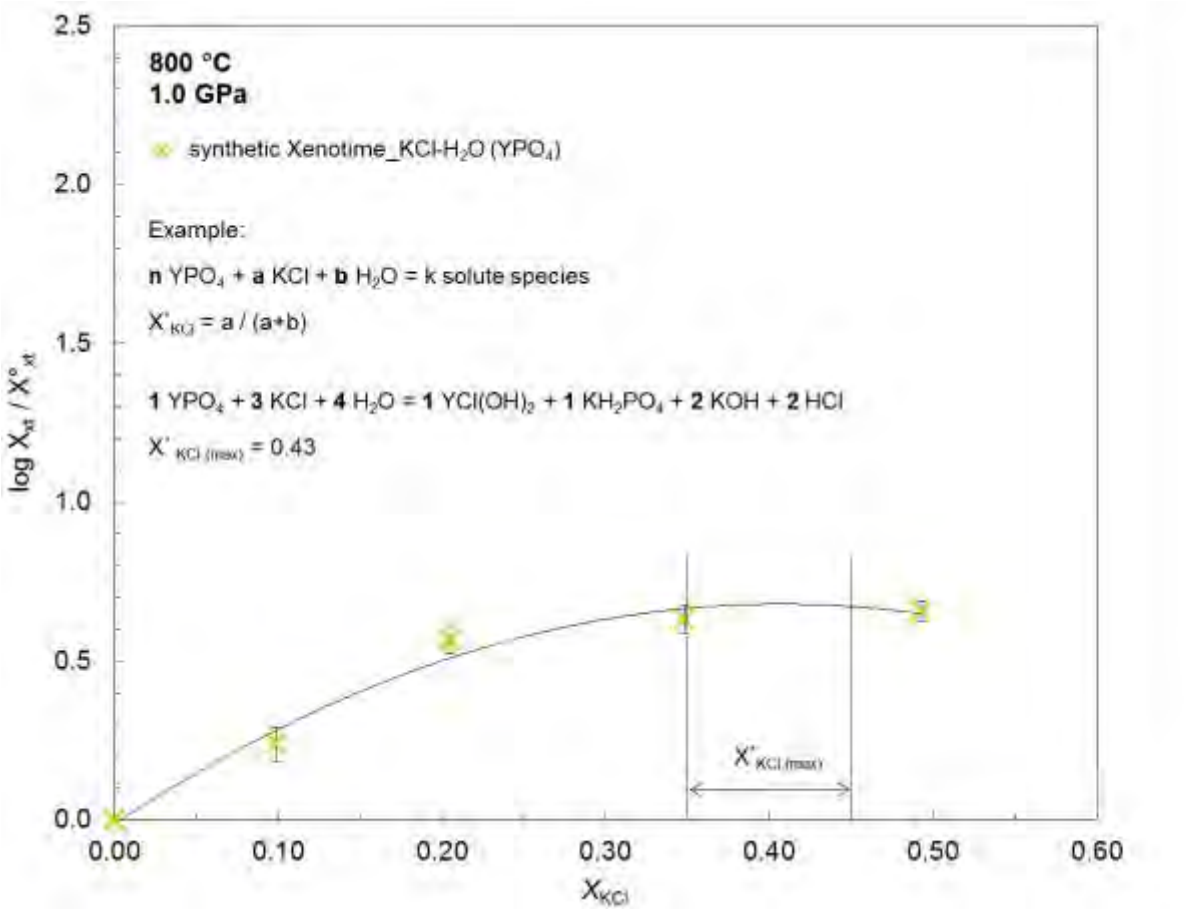
800 °C
1.0 GPa
synthetic Xenotime_KCl-H2O (YPO4)
Example:
n YPO4 + a KCl + b H2O = k solute species
X'KCl = a / (a+b)
1 YPO4 + 3 KCl + 4 H2O = 1 YCl(OH)2 + 1 KH2PO4 + 2 KOH + 2 HCl
X'KCl (max) = 0.43
log Xxt / X°xt
XKCl
X'KCl (max)
2.5
2.0
1.5
1.0
0.5
0.0
0.00
0.10
0.20
0.30
0.40
0.50
0.60

Figure 6b.